Supporting Information

Kodack et al. 10.1073/pnas.1216078109

SI Materials and Methods

Cranial Window, Intravital Multiphoton Microscopy, and Tumor Volume Calculation. Cranial windows were implanted into nude mice as previously described (1). Intravital imaging of normal and angiogenic vessel morphology was performed using custom-built multiphoton laser scanning microscopy instrumentation. To contrast-enhance functional blood vessels, angiography was performed after i.v. injection of 0.1 mL rhodamine-dextran (10 mg/mL, 2,000 kDa). For intravital tumor volume calculation, BT474-*Gaussia* luciferase (Gluc) tumors were measured twice a week by intravital fluorescent microscopy. Using an in-house MATLAB (MathWorks) program, an ellipse was fitted to the cerulean fluorescent protein (tumor) signal and the short and long axes were calculated. Tumor volume was calculated based on a half-ellipse, using the following equation:

$$\text{Tumor volume} = ((\text{long axis}) \times (\text{short axis}) \times ((\text{long axis} + \text{short axis})/2) \times \pi/6)/2$$

MRI. MRI-based measurement of tumor growth was performed similar to the technique used by Kamoun et al. (2). All experiments were performed on a 9.4-T magnet (Magnex Scientific Ltd.) equipped with a gradient coil with a 60-mm inner diameter (Resonance Research) and interfaced with an MRI console (Bruker BioSpin). The gradient coil has a maximum strength of 1,500 mT/m and a rise time of 100 μs. Images were acquired using a home-built mouse head birdcage coil. Mice were positioned on a custom-made mouse cradle and anesthetized with 1.5% (vol/vol) isoflurane in a 50:50 O_2/medical air mixture with total flow rate of 1,200 mL/min. T2-weighted RARE images were acquired to assess the tumor volume. The image acquisition parameters were as follows: echo time/repetition time = 10/3,000 ms; rapid acquisition relaxation enhanced factor = 16, four averages; field of view = 1.92 cm; matrix = 128 × 128 (in-plane resolution = 150 μm); 0.5-mm slice thickness; and 11 image slices. Tumor volume was determined manually from the T2 hyperintense tumor regions of the brain.

Bioluminescence Imaging. Individual animals were anesthetized, and bioluminescence imaging (BLI) was performed immediately after retroorbital injection of coelenterazine (CTZ) solution (at a concentration of 4 mg/kg of body weight). An In Vivo Imaging System (IVIS Lumina II; Caliper Life Sciences) was used for bioluminescence image recording. The image acquisition time was 30 s at a precise 30-s time point after retroorbital injection. (Because Gluc has flash kinetics, imaging at a consistent time after CTZ injection is critical.) Postprocessing and quantification were performed using Living Image Software 3.0 (Caliper Life Sciences) coupled to the IVIS system. Image analysis was done similar to the technique used by Chung et al. (3).

Ex Vivo Multispectral Fluorescent Imaging. The same mice used for the MRI analysis, bearing BT474-Gluc tumors treated with either control IgGs or the combination of trastuzumab and DC101, were killed immediately after the last imaging sequence. The entire brain was collected and fixed in 4% formaldehyde. After 24 h, the brain was sectioned into 1-mm slices. The tumor area was revealed in each section by spectral unmixing using the Maestro System (Cambridge Research and Instrumentation). Tumor volume was calculated by integration of the tumor areas, knowing that each section is 1 mm thick.

Histology and Immunostaining. Before embedding tissues in paraffin, mouse brains were fixed for 8 h in 4% formaldehyde in PBS at 4 °C, followed by washes in PBS and storage at 4 °C. Phosphorylation of human epidermal growth factor receptor-2 (HER2) was visualized with an anti–phospho-HER2 antibody (Tyr1221/Tyr1222, clone 6B12; Cell Signaling Technology) diluted at 1:320 in SignalStain Diluent (Cell Signaling Technology) and incubated overnight, followed by incubation with SignalStain Boost IHC Detection Reagent (HRP, rabbit; Cell Signaling Technology) for 1 h at room temperature (RT). Identification of proliferating cells was done using a Ki67 antibody (clone MIB-1; Dako) supplied at the working concentration and incubated for 1 h at RT, followed by incubation with mouse EnVision polymer (Dako) for 30 min at RT. Identification of apoptotic cells was accomplished using an antibody to cleaved caspase 3 (clone 5A1E; Cell Signaling Technology) diluted 1:50 and incubated overnight. Liquid DAB+ (Dako) was used to detect HRP-conjugated anti-mouse and anti-rabbit secondary antibodies, followed by mounting in Permount.

Western Blotting. Tumor tissues were resuspended in 1% Nonidet P-40 lysis buffer (15 mM Tris, 10 mM EDTA, 10 mM EGTA) with protease and phosphatase inhibitors, and incubated on ice for 10 min. After cell lysis, lysates were centrifuged at 14,000 rpm (~18,000 × *g*) for 10 min at 4 °C. The protein concentration of the supernatant was measured before boiling in Laemmli buffer. Western blot analysis was conducted after separation by SDS/PAGE electrophoresis and transferred to nitrocellulose membranes. Immunoblotting was performed according to the antibody manufacturers' recommendations. The anti–phospho-HER2, anti-pospho Akt, anti-Akt, anti-phospho-ERK, and anti-ERK antibodies were obtained from Cell Signaling Technologies, and the anti-HER2 antibody was obtained from Calbiochem (EMD Chemicals).

Fluorescence-Activated Cell Sorting and Quantification of Tumor Natural Killer Cells, and Depletion of Natural Killer Cells. For the quantification of natural killer (NK) cells within the tumor, tumor-bearing mice were intracardially perfused with PBS. Tumor tissues were harvested, minced, and digested at 37 °C for 60 min with complete DMEM containing collagenase type 1A (1,500 U/mL), hyaluronidase (1,000 UI/mL), and DNase (2 mg/mL). The digestion mixtures were filtered through 70-μm cell strainers. Single-cell suspensions were incubated with rat anti-mouse CD16/CD32 monoclonal antibodies and then stained, washed, and resuspended in cold buffer (1% BSA, 0.1% NaN_3 in PBS). 7-Aminoactinomycin D (eBioscience) was added to the stained tubes (5 μL per tube) to exclude dead cells. Flow cytometry data were acquired on an LSRII flow cytometer (Becton Dickinson Biosciences) and analyzed with FACSDiva software (Becton Dickinson Biosciences). Appropriate fluorochrome-conjugated, isotype-matched control IgGs were used in all experiments. The anti-mouse antibodies CD45-phycoerythrin (PE)-Cy7 and NK1.1-PE (Becton Dickson Biosciences) were used. For the depletion of NK cells in mice, the NK1.1 antibody (clone PK136; BioXCell) was administered at a concentration of 4 mg/kg of body weight twice a week by i.p. injection. The control for the NK1.1 antibody was 4 mg/kg of body weight of a nonspecific mouse IgG (Jackson ImmunoResearch Laboratories, Inc.).

In Vitro Cell Growth Assay. A total of 3,000 BT474-Gluc cells were seeded in RPMI + 5% FBS in a 96-well plate and allowed to adhere overnight. Cells were treated the following day, and growth was

measured 5 d after treatment addition. Cell growth was measured using the CellTiter-Glo Luminescent Cell Viability Assay (Promega).

Statistical Analysis. Data are expressed as the mean ± SEM unless otherwise noted. The principal statistical test was a one-way ANOVA, and Tukey's posttest was used to compare all pairs of columns. A *t* test (two-tailed with unequal variance) was used when only two variables were present in the analysis. Significant differences in tumor growth were accomplished by determining the time it took (in days) to reach a specific blood Gluc activity (specific for each experiment and illustrated on the tumor growth curve graph) (Fig. 2 *A* and *B*, Fig. 6 *A* and *B*, and Fig. S8*D*). The survival curves were estimated using the Kaplan–Meier method, and the median survival day was used when determining statistical difference. Statistical significance is defined throughout the main text and figure legends. GraphPad Prism was used for all statistical analysis.

1. Yuan F, et al. (1994) Vascular permeability and microcirculation of gliomas and mammary carcinomas transplanted in rat and mouse cranial windows. *Cancer Res* 54 (17):4564–4568.
2. Kamoun WS, et al. (2009) Edema control by cediranib, a vascular endothelial growth factor receptor-targeted kinase inhibitor, prolongs survival despite persistent brain tumor growth in mice. *J Clin Oncol* 27(15):2542–2552.
3. Chung E, et al. (2009) Secreted Gaussia luciferase as a biomarker for monitoring tumor progression and treatment response of systemic metastases. *PLoS ONE* 4(12): e8316.

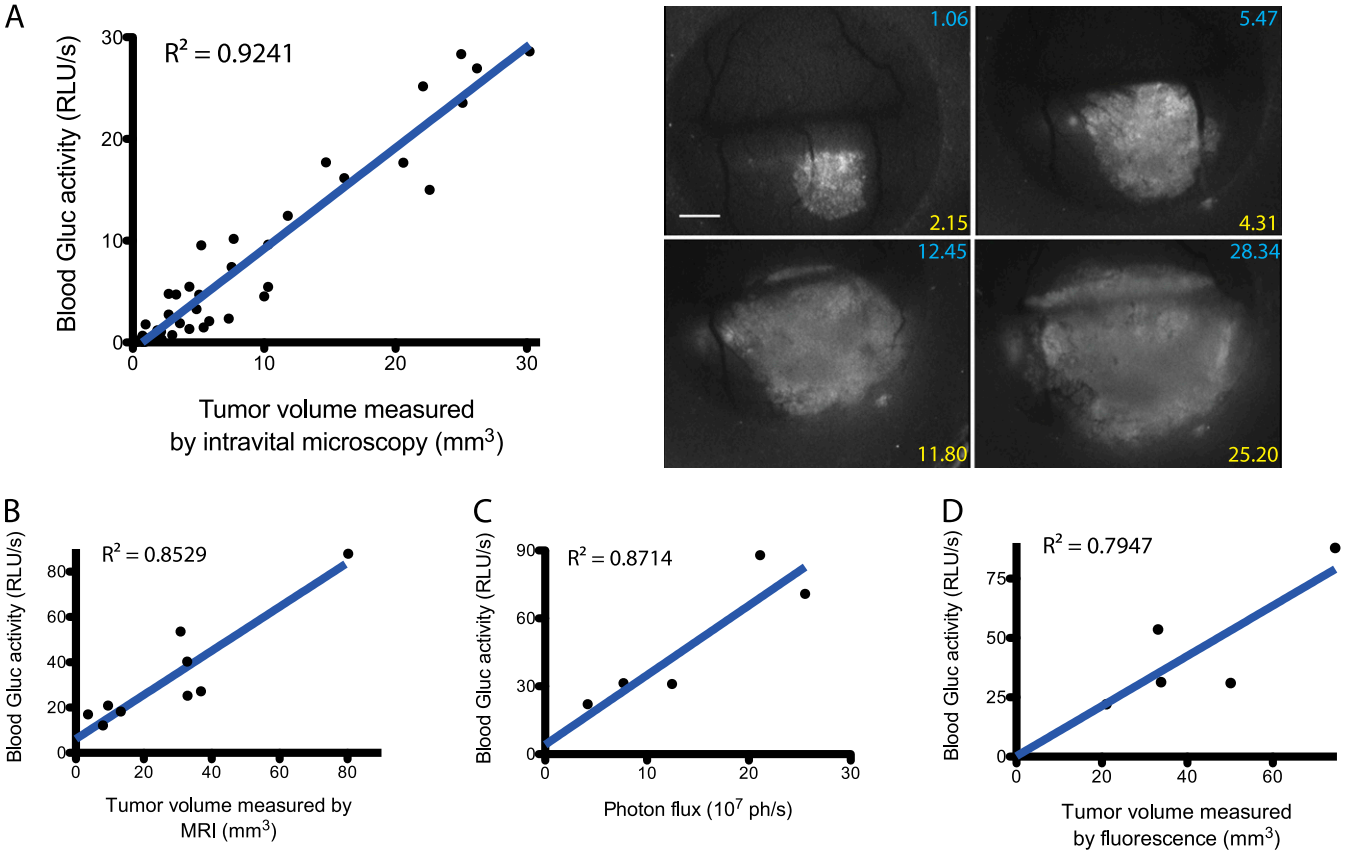

Fig. S1. Correlation of blood Gluc activity and tumor volume measurements. (*A*) Correlation of blood Gluc activity and tumor volume, measured using intravital microscopy. BT474-Gluc cells were injected into the brain parenchyma of mice with a cranial window. Tumors were imaged through the cranial window using a fluorescent microscope, and tumor length and width were obtained, from which volume was calculated. Blood was collected from the mice at the time of imaging. (*Left*) Blood Gluc activity is plotted against tumor volume, and linear regression analysis was performed using Prism software. Representative pictures are shown (*Right*), and inserted numbers correspond to the blood Gluc activity (*Upper*, blue) and the calculated tumor volume (*Lower*, yellow) ($n = 8$ mice, 44 separate measurements). (Scale bar: 1 mm.) (*B*) Correlation of blood Gluc activity and tumor volume, measured with MRI; representative images are shown in Fig. 3*A* (control-treated mice only; $n = 4$ mice, 9 separate measurements). (*C*) Correlation of blood Gluc activity and tumor volume, measured with bioluminescence imaging; representative images are shown in Fig. 3*B* (control-treated mice only; $n = 5$ mice). (*D*) Correlation of blood Gluc activity and tumor volume, measured by ex vivo multispectral fluorescent microscopy; representative images are shown in Fig. S2 (control-treated mice only; $n = 5$ mice).

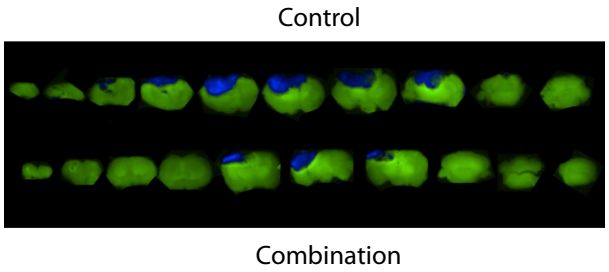

Fig. S2. Representative images of control-treated (*Upper*) or trastuzumab and DC101-treated (*Lower*) brain sections. Spectral unmixing reveals tumor (cerulean fluorescent protein, blue) and normal (autofluorescence, green) tissue. Each section is 1 mm thick. Images were obtained with the Maestro System.

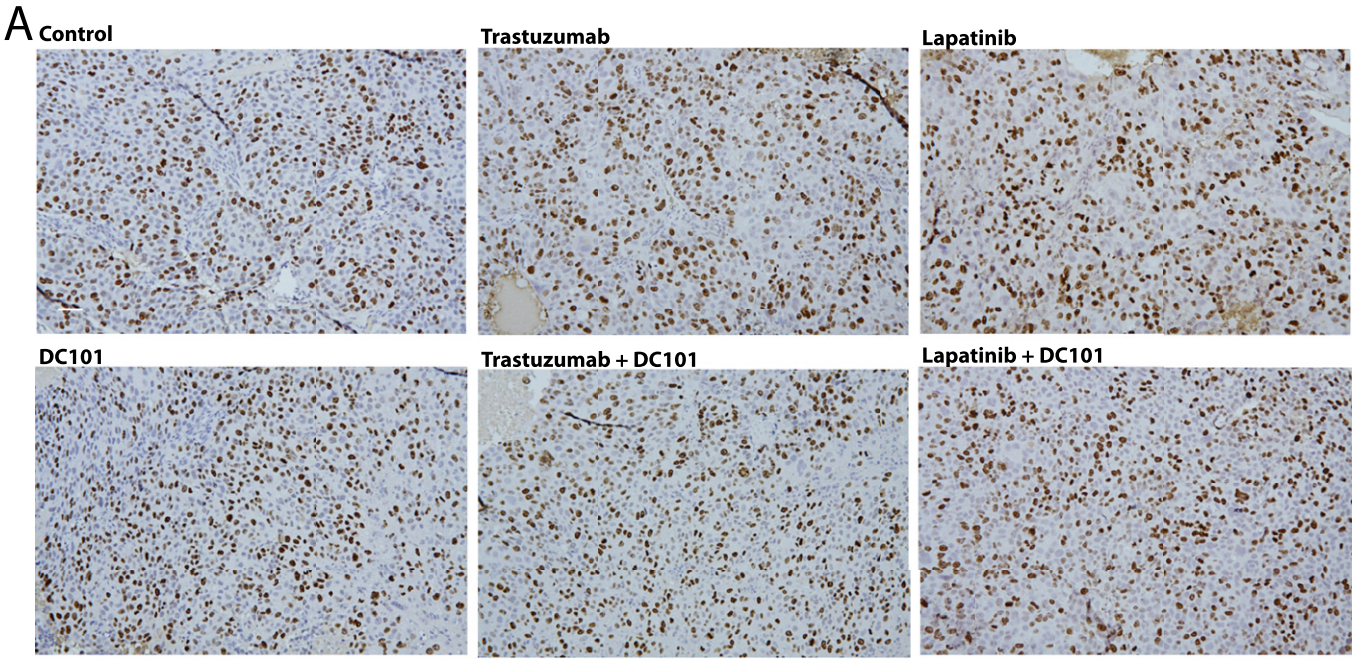

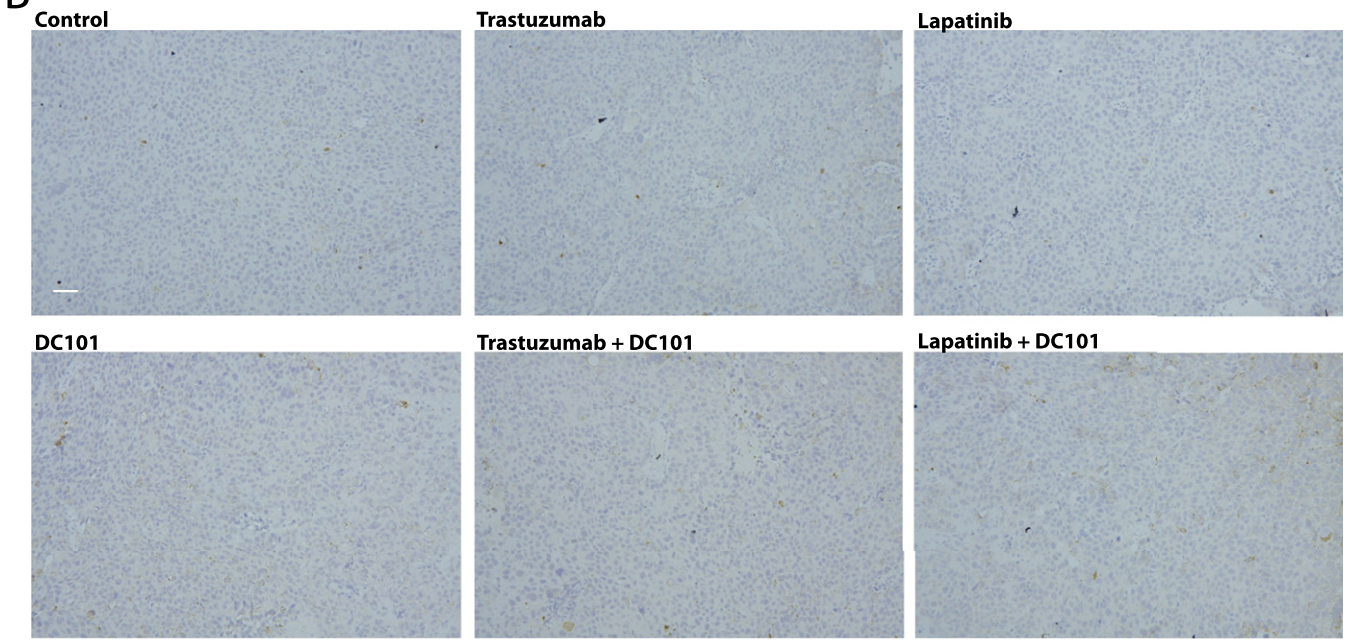

Fig. S3. Effect of the indicated treatments on cell proliferation and apoptosis. Immunohistochemical analysis of Ki67 (*A*) or cleaved caspase 3 (*B*) staining in tumor tissues harvested 15 d after the initiation of treatment and paraffin-embedded. (Scale bars: 50 μm.)

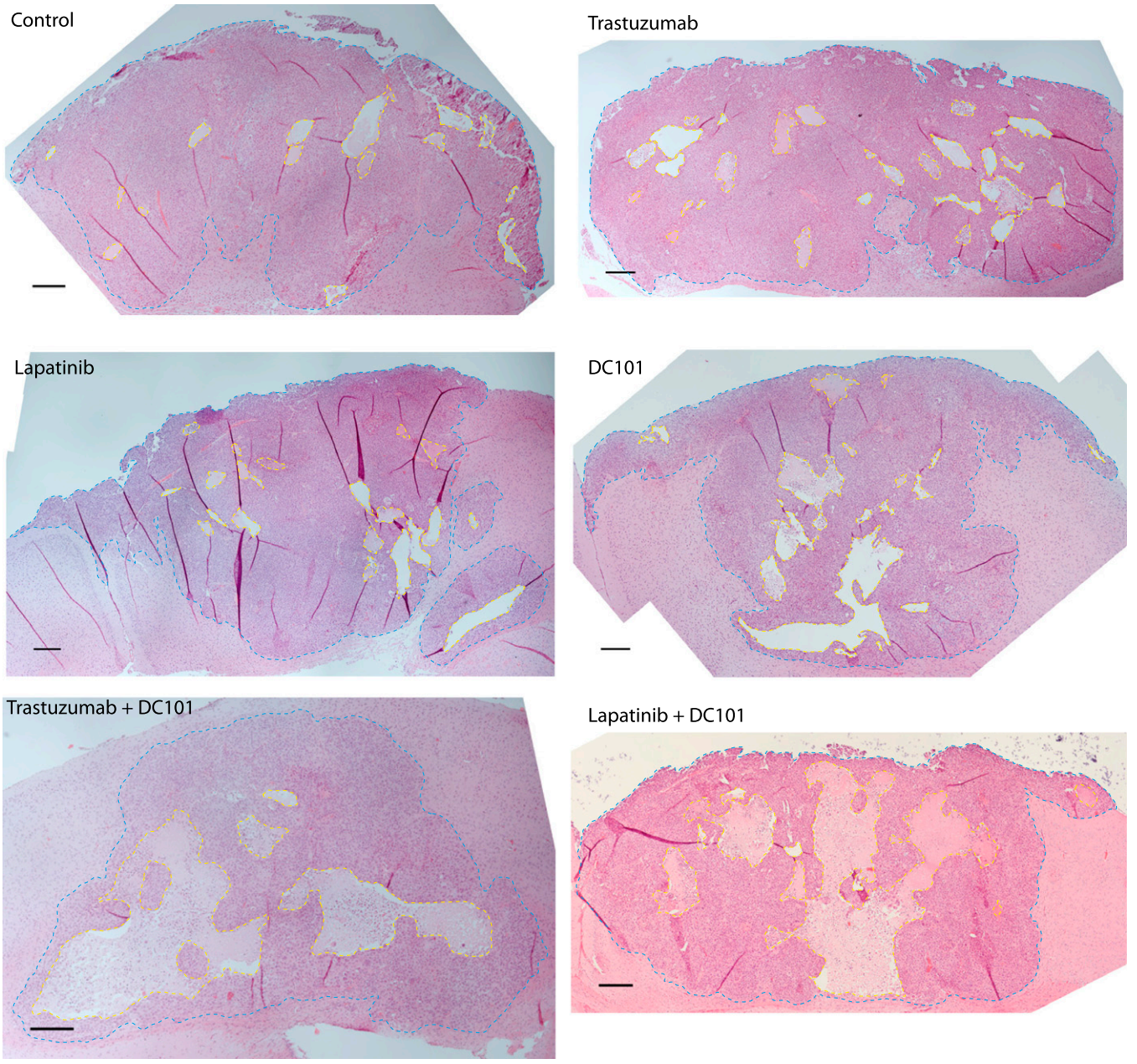

Fig. S4. Representative H&E-stained sections of BT474-Gluc brain metastatic tumor tissues used for the quantification of the necrotic area in Fig. 4. The borders of total tumor area and necrotic regions are highlighted in dotted blue and yellow lines, respectively. (Scale bars: 250 μm.)

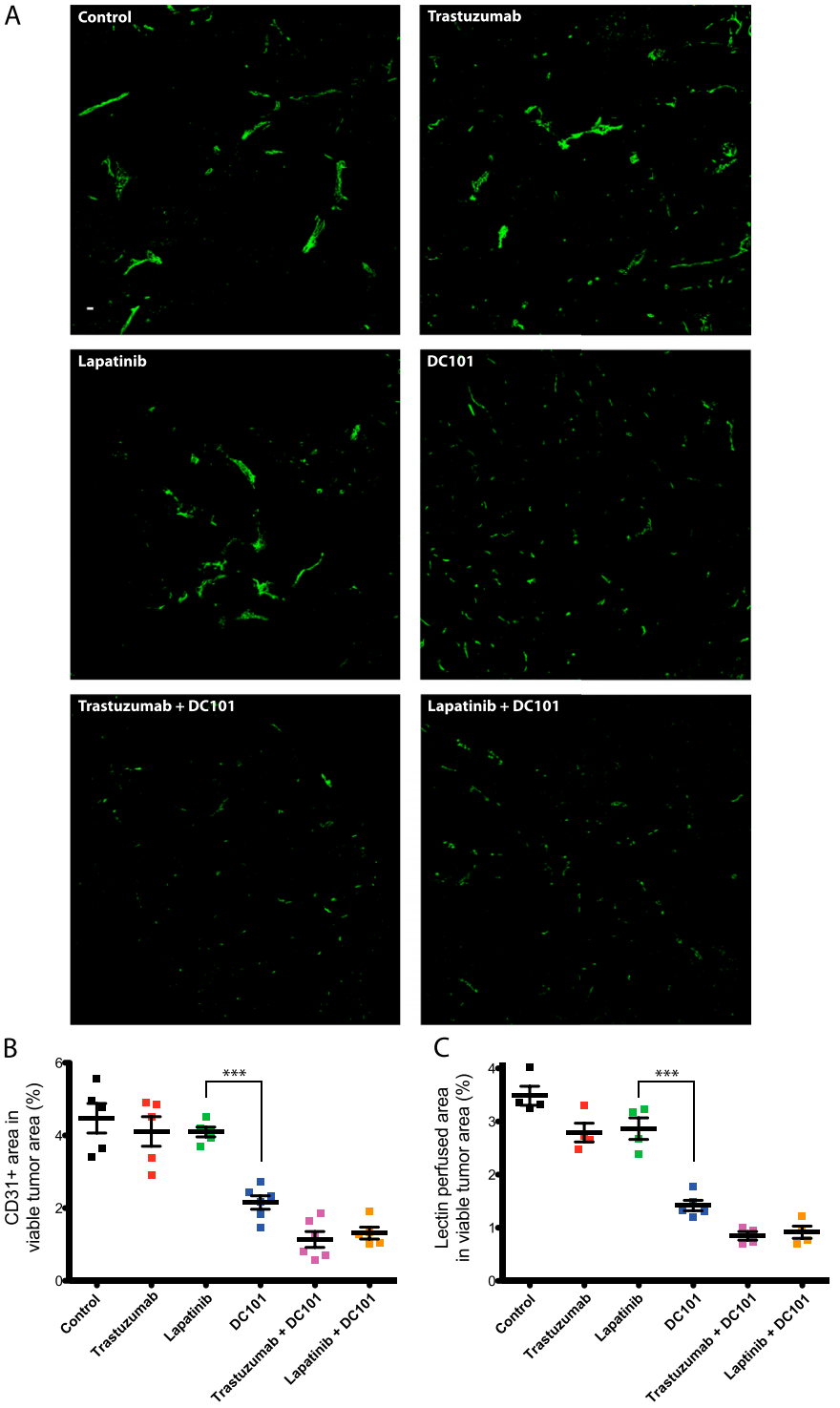

Fig. S5. Effect of the indicated treatments on the tumor vasculature. (*A*) Representative images of lectin-positive endothelial cells in the viable tumor tissue 15 d after the start of treatment. (Scale bar: 100 μm.) (*B* and *C*) Effects of the indicated treatments on blood vessels in BT474-Gluc tumors 8 d after treatment initiation. (*B*) Percentage of CD31-positive blood vessel area within the viable tumor regions for each tumor was calculated using an in-house MATLAB program. (*C*) Before euthanasia, mice were injected with 2.5 μg of biotinylated-lectin per gram of body weight into the heart and allowed to circulate for 5 min. The area of lectin-positive blood vessels in the viable tumor regions for each tumor was calculated using an in-house MATLAB program. ***$P < 0.001$. DC101 vs. trastuzumab and DC101 or lapatinib and DC101, not statistically different.

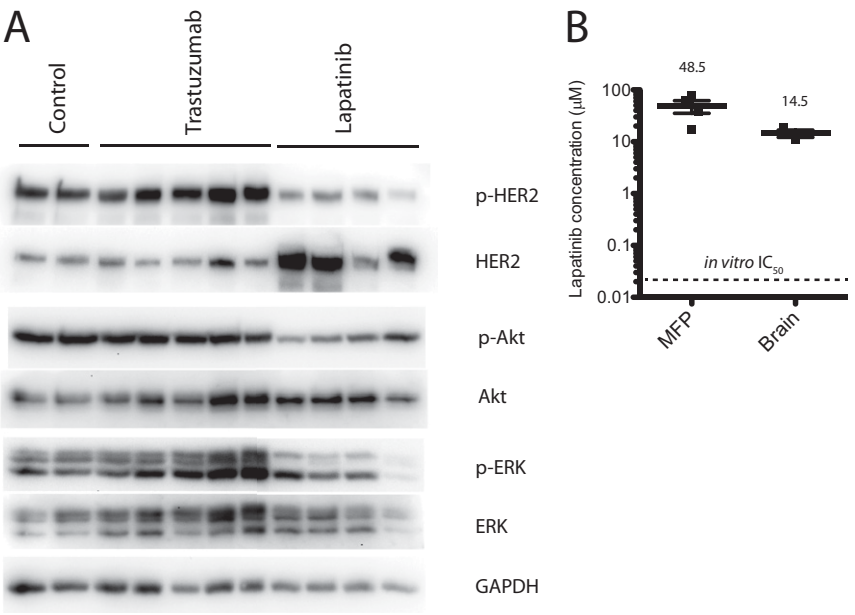

Fig. S6. Effect and delivery of the indicated treatments. (*A*) Effect of trastuzumab and lapatinib treatment on HER2, AKT, and ERK phosphorylation in BT474-Gluc tumors growing in the brain 3 d after treatment initiation. Tumor tissues were collected 2 h after the last treatment. Western blotting illustrates levels of HER2, AKT, and ERK phosphorylation and corresponding total protein levels, as well as for GAPDH as a loading control. (*B*) Concentration of lapatinib in BT474-Gluc mammary fat pad and brain metastatic tumors (not statistically different). The dotted line marks the reported in vitro IC_{50} of lapatinib for BT474 cells.

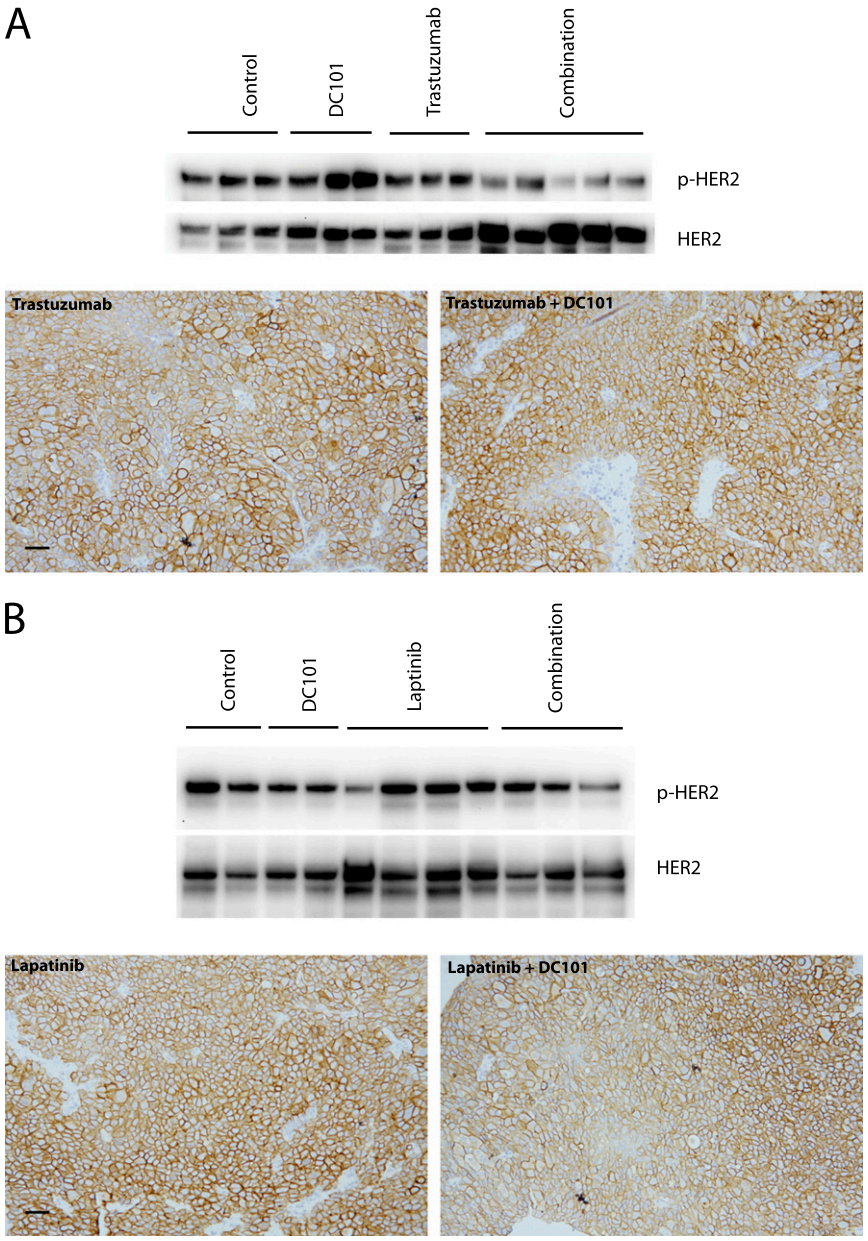

Fig. S7. Effect of anti-HER2 treatments alone or in combination with anti-VEGFR2 treatment on HER2 phosphorylation (p-HER2). Brain metastatic BT474-Gluc tumor tissues were harvested 15 d after the initiation of treatment with trastuzumab monotherapy and in combination with DC101 (*A*) or lapatinib monotherapy and in combination with DC101 (*B*). Tissues were either snap-frozen for protein lysis and Western blotting (*Upper*) or paraffin-embedded for immunohistochemistry (*Lower*). (Scale bars, 50 μm.)

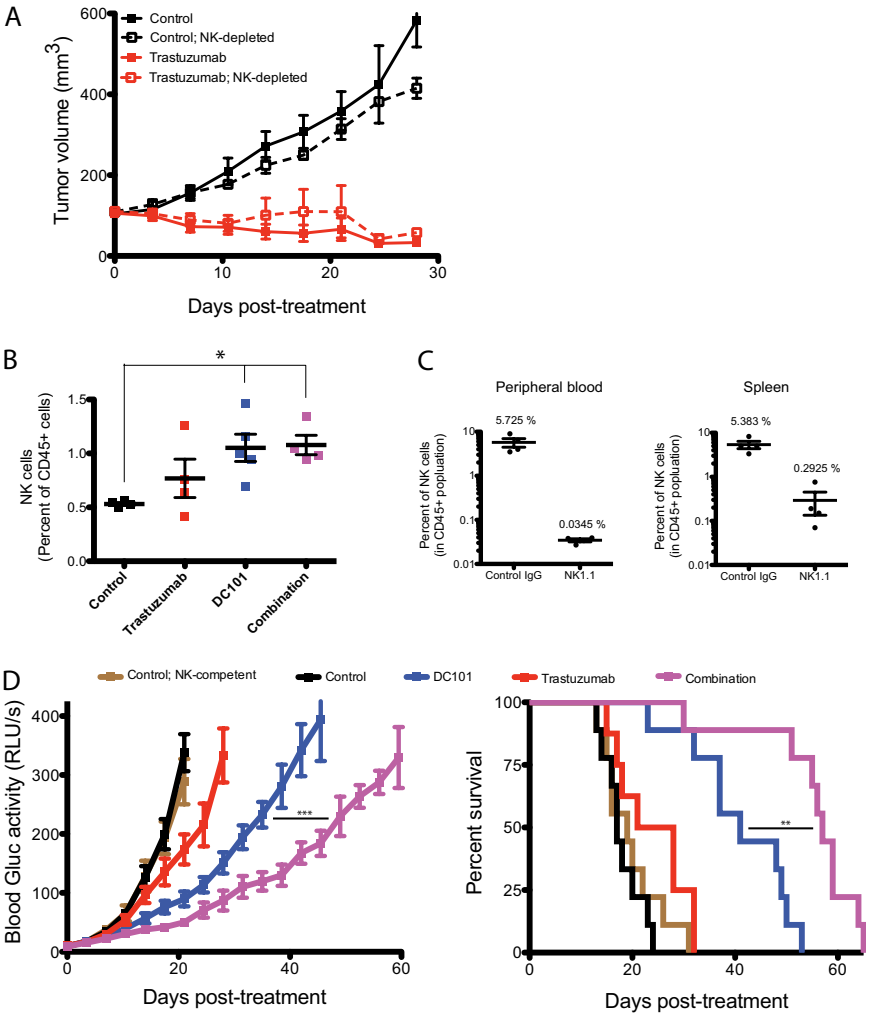

Fig. S8. Role of NK cells in mammary fat pad and brain metastatic breast cancers treated with anti-HER2 and/or anti-VEGFR2 agents. (*A*) Effect of the depletion of NK cells on control-treated (dotted black line) and trastuzumab-treated (dotted red line) BT474-Gluc mammary fat pad growth. Nude mice were treated with the NK1.1 antibody at the time of treatment initiation. Tumor growth curves for control-treated (solid black line) and trastuzumab-treated (solid red line), NK cell-competent mice are shown ($n = 6$ mice). (*B*) FACS analysis of NK1.1-positive and CD45-positive cells within brain metastatic BT474-Gluc tumors 14 d after treatment initiation. $^{*}P < 0.05$. (*C*) Effect of the NK1.1 antibody (clone PK136) on the presence of NK cells in the peripheral blood (*Left*) and spleen (*Right*). $P < 0.01$. (*D*) Effect of the depletion of NK cells on control-treated (black), trastuzumab-treated (red), DC101-treated (blue), and trastuzumab and DC101-treated (magenta) BT474-Gluc brain metastatic growth. Nude mice were treated with the NK1.1 antibody at the time of trastuzumab and/or DC101 treatment initiation. A tumor growth curve plot (*Left*) and Kaplan–Meier survival plot (*Right*) are shown for each treatment group. Tumor growth and survival curves for control-treated, NK cell-competent mice are shown in brown ($n = 8$–9 mice). $^{**}P < 0.01$; $^{***}P < 0.001$.

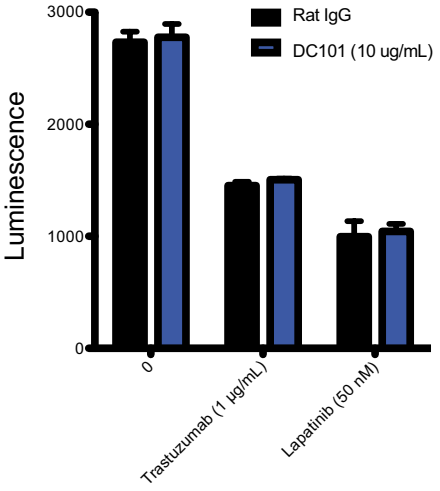

Fig. S9. Effect of the combination of anti-HER2 and antimurine VEGFR2 agents on BT474-Gluc growth in vitro. BT474-Gluc cells were seeded in triplicate in a 96-well plate; allowed to adhere; and treated with the indicated concentrations of control IgG, DC101, trastuzumab, and/or lapatinib. After 5 d of treatment, cell growth was measured using the CellTiter-Glo Luminescent Cell Viability Assay. There was no significant difference between rat IgG and DC101 in the absence of an HER2 inhibitor, in the presence of trastuzumab, or in the presence of lapatinib. The graph is a representative of three separate experiments.

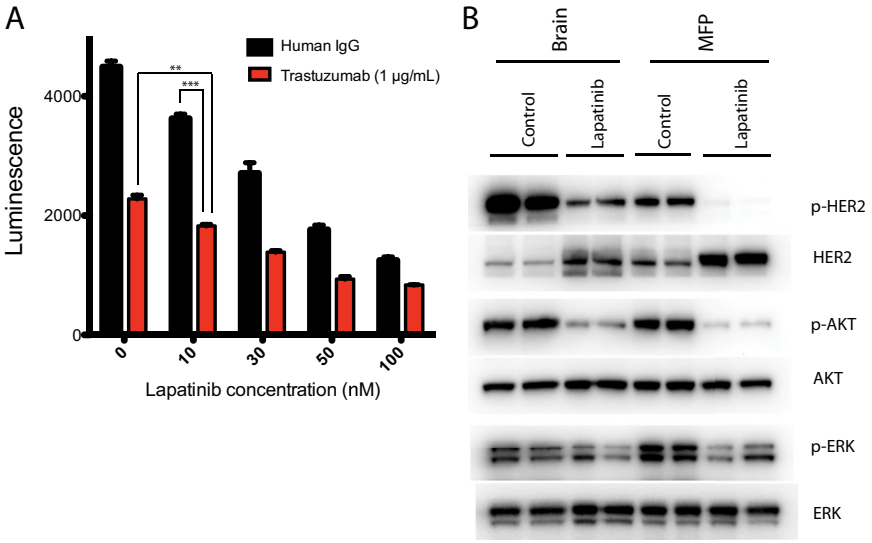

Fig. S10. Effect of two anti-HER2 therapies compared with one and the differences between tumor cells growing in the mammary fat pad or brain. (*A*) Effect of the combination of two anti-HER2 therapies on BT474-Gluc growth in vitro. BT474-Gluc cells were seeded in triplicate in a 96-well plate; allowed to adhere; and treated with the indicated concentrations of control IgG, trastuzumab, and/or lapatinib. After 5 d of treatment, cell growth was measured using the CellTiter-Glo Luminescent Cell Viability Assay. $^{**}P < 0.01$; $^{***}P < 0.001$. The graph is representative of three separate experiments. (*B*) Effect of lapatinib on HER2, AKT, and ERK phosphorylation in BT474-Gluc tumors growing in the brain (*Left*) or mammary fat pad (MFP; *Right*). Tumor tissues were collected 3 d after treatment initiation, and Western blotting was performed to quantify phosphorylation (p) and corresponding total protein levels.